This paper is a post-print of a paper submitted to and accepted for publication in IET Renewable Power Generation and is subject to Institution of Engineering and Technology Copyright. The copy of record is available at IET Digital Library.

ENHANCED AC VOLTAGE AND FREQUENCY CONTROL OF OFFSHORE MMC STATION FOR WIND FARM CONNECTION

Yiran Jing [1*], Rui Li [1], Lie Xu [1], Yi Wang [2]

[1] Department of Electronic and Electrical Engineer, University of Strathclyde, 99 George St, Glasgow, UK

[2] North China Electric Power University, China

[*] yiran.jing@strath.ac.uk

Abstract: Connecting large offshore wind farms using HVDC transmission systems based on modular multilevel converter (MMC), the offshore AC voltage and frequency are regulated by the offshore MMC station and are important for the stable wind power generation and transmission. This paper proposes an enhanced AC voltage and frequency control strategy of the offshore MMC for wind farm integration, where an additional frequency loop is used to improve its AC voltage and frequency controllability. A fault current injection control is also proposed, where the offshore MMC station actively provides fault currents during an offshore AC fault to enable overcurrent protection for the network. To ride-through onshore AC faults, a DC voltage dependent AC voltage controller is introduced to actively reduce the offshore AC voltage during an onshore AC fault to alleviate the DC overvoltage of the HVDC system. Simulation results in normal operation and during offshore and onshore faults confirm the feasibility of the proposed control scheme.

1. Introduction

To reduce the usage of fossil fuels and meet the energy demand, offshore wind energy has developed rapidly in the past few years due to low turbulence and high average wind speed [1, 2]. High voltage direct current (HVDC) transmission system based on modular multilevel converter (MMC) is likely to be used for integrating future long distance offshore wind farms due to the improved controllability and superior system performances [2-8]. The offshore MMC station forms the AC power system in large offshore wind farms, which is typically weak and exhibits voltage oscillation or harmonic resonance in the event of faults [9-12]. Stable AC voltage and frequency control is thus a prerequisite for the transmission of offshore wind energy.

Fixed frequency control is the most common approach to regulate the AC voltage of offshore network. With fixed offshore frequency, the *q*-axis output voltage reference of the MMC is directly set at zero while a PI controller is used to regulate the *d*-axis voltage, thereby the offshore voltage magnitude [13]. The controller is implemented in *abc* reference frame in [14] to avoid synchronous *dq* transformation and proportional-resonant (PR) controllers are utilized to ensure zero steady-state error for sinusoidal voltages. In [15], offshore grid three-phase voltages are added to the output of the PR controllers as feedforwards to improve the dynamics of offshore voltage controller. However, as these control schemes only contain voltage control loop and do not have current controllability, system performance of the offshore MMC stations, especially during severe offshore AC faults, cannot be guaranteed.

To limit fault currents and avoid damage of offshore MMC station, three-phase currents are measured in [16] to adjust the voltage control loop reference. If the currents are out of the predefined range, the offshore voltage is reduced accordingly in order to decrease the MMC output currents.

A decoupled current controller is further introduced in [6, 9, 17, 18], which are bypassed during normal operation. Once the currents are out of the predefined threshold, the current controllers are trigged to limit the output currents and MMCs are switched to current control mode. After fault clearance, MMCs are switched back to the voltage control mode. However, the switching between voltage and current control modes can potentially lead to transient current surge.

The cascaded control structure with outer voltage loop and inner current loop is used in [19] to control both offshore voltage and current and avoid the control mode switching. Based on the cascaded controller, an extended limitation method for the converter current references are then proposed in [20] to effectively utilize the MMC capability in grid-forming operating mode, considering unbalanced conditions. However, the offshore frequency is fixed in the aforementioned control approaches and the

This paper is a post-print of a paper submitted to and accepted for publication in IET Renewable Power Generation and is subject to Institution of Engineering and Technology Copyright. The copy of record is available at IET Digital Library.

offshore frequency flexibility is not utilized. A DC voltage frequency droop control is proposed in [21] to adjust the offshore frequency proportional to the HVDC voltage variation in order to mirror the onshore frequency deviation into the offshore network. However, the interaction between the frequency and the voltage is not investigated.

Onshore network fault is also a serious problem for HVDC connected offshore wind farms. Faults on onshore AC system could prevent the HVDC onshore receiving end from exporting power generated by the WF leading to potential DC over voltage. To enable the continuous operation of the HVDC link, the excess power from the WF has to be dissipated or the power generated by the wind turbines be reduced. In [22], a method of De-loading which rapidly reduces the generator torque when faults are detected, is used. In [12], the offshore HVDC converter increases the offshore AC frequency upon the detection of DC voltage rise on the HVDC link, and the wind turbines subsequently reduce the output power after detecting the increased frequency. Using damping resistors on DC link of the HVDC system has also been used for dissipating the excess power [23].

Offshore AC fault is another challenge for the continuous operation of offshore wind farms. During offshore AC fault, the AC currents of the voltage source converters (VSCs) connected with the offshore network are simply controlled at zero in [24] without considering the need for the operation of the protection relays. In [25], a fault current limiter is presented to reduce the MMC output voltage after offshore faults and limit the fault currents. However, how to detection the fault is not addressed. Reference [26] proposes a coordinated voltage control scheme which enables the offshore VSCs to provide fault currents after offshore AC fault to support the offshore grid. However, communication is required between the offshore HVDC stations and wind turbine (WT) converters.

This paper proposes an enhanced AC voltage and frequency control of offshore MMC station connected with wind farms. Considering the operating principle of the phase-locked loop (PLL), the offshore frequency flexibility is utilized to improve the offshore voltage controllability. With the proposed control scheme, the fault current providing capability is investigated to enable overcurrent protection during offshore AC faults. To ride-through onshore AC faults, a DC voltage dependent AC voltage controller is introduced to the offshore MMC station to actively reduce the offshore AC voltage and alleviate DC overvoltage of the HVDC system.

This paper is organized as follows. The layout of the MMC-HVDC system for connecting offshore wind farms is presented in Section 2 and Section 3 describes the basic control of the offshore MMC. The enhanced AC voltage and frequency control is proposed in Section 4, and MMC controllers for contributing fault current during offshore AC faults and riding through onshore AC faults are presented. The proposed control scheme is assessed using simulations in Section 5, considering normal operation, offshore and onshore AC faults. Finally, conclusion is drawn in Section 6.

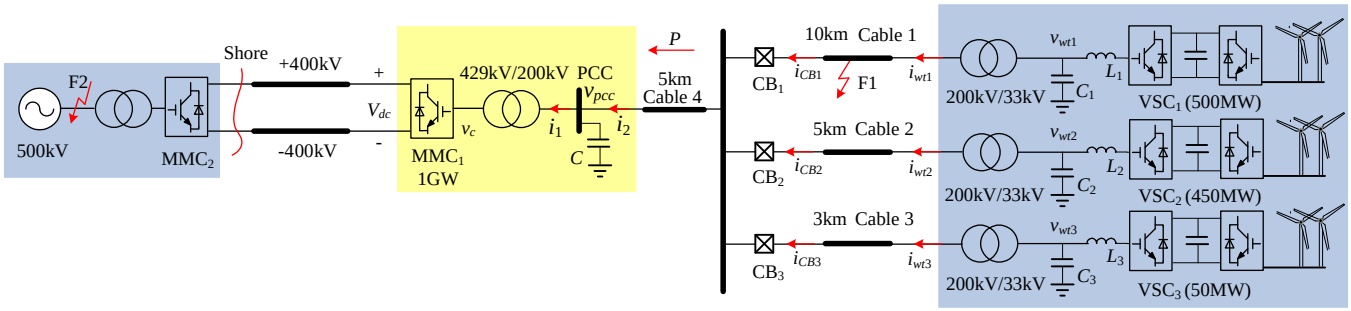

Fig. 1. *System structure with lumped wind turbine cluster models.*

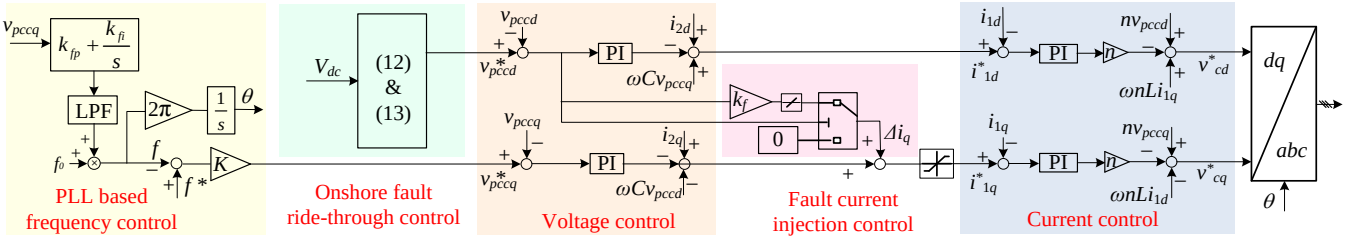

Fig. 2. *Enhanced voltage and frequency control strategy of the offshore MMC station.*

2 System structure

The considered offshore wind farm connected with an MMC-HVDC is schematically shown in Fig. 1, where three lumped wind turbine models are used to represent different wind turbine clusters with a total power rating of 1000 MW. A symmetrical monopole HVDC system with rated DC voltage of ±400 kV is considered in this paper. AC circuit breakers (CB_1, CB_2, and CB_3, Fig. 1) are equipped at the end of the cluster cables to isolate the fault branch and enable

This paper is a post-print of a paper submitted to and accepted for publication in IET Renewable Power Generation and is subject to Institution of Engineering and Technology Copyright. The copy of record is available at IET Digital Library.

continuous operation of the healthy wind turbines in the event of a fault in the offshore AC network.

The offshore station MMC_1 controls the AC voltage and frequency of the offshore network while the onshore station MMC_2 regulates the DC voltage of the HVDC link. The grid-side converters of WTs based on permanent magnet synchronous generators operate on power control mode to transmit wind energy to the offshore grid. The WT DC voltage is regulated by the generator-side converters.

3 Basic control of offshore MMC station

The offshore MMC station works as a grid-forming converter to establish the offshore AC network frequency and voltage, as well as balancing the transmitted active power between WTs and the offshore network. The offshore MMC typically contains an outer AC voltage control loop and an inner current loop to provide fast system dynamics and to enable MMC fault current limiting capability during offshore AC faults, as shown in Fig. 2.

3.1 Inner current loop

For the offshore station MMC_1 shown in Fig. 1, the current loop dynamics in the *dq* reference frame where the *d*-axis is fixed to the PCC voltage v_{pcc} are expressed as

$$\begin{bmatrix} v_{cd} \\ v_{cq} \end{bmatrix} = \begin{bmatrix} 0 & n\omega L \\ -n\omega L & 0 \end{bmatrix} \begin{bmatrix} i_{1d} \\ i_{1q} \end{bmatrix} - \begin{bmatrix} nL & 0 \\ 0 & nL \end{bmatrix} \frac{d}{dt} \begin{bmatrix} i_{1d} \\ i_{1q} \end{bmatrix} + n \begin{bmatrix} v_{pccd} \\ v_{pccq} \end{bmatrix} \quad (1)$$

where ω is the angular frequency of the offshore network; L is the transformer leakage inductance; i_{1d} and i_{1q} are the MMC *dq* currents; v_{cd} and v_{cq} are MMC output *dq* voltages; v_{pccd} and v_{pccq} are *dq* PCC voltages; and n is the transformer ratio.

With proportional-integral (PI) regulators, the current control loop as illustrated in Fig. 2 is described as:

$$\begin{cases} v_{cd}^* = nv_{pccd} + \omega nLi_{1q} - n\left[k_{ip}(i_{1d}^* - i_{1d}) + k_{ii}\int (i_{1d}^* - i_{1d})dt\right] \\ v_{cq}^* = nv_{pccq} - \omega nLi_{1d} - n\left[k_{ip}(i_{1q}^* - i_{1q}) + k_{ii}\int (i_{1q}^* - i_{1q})dt\right] \end{cases}. \quad (2)$$

3.2 Outer AC voltage loop

The outer AC voltage loop sets the current references and its dynamics in the *dq* reference frame are expressed as:

$$\begin{bmatrix} i_{1d} \\ i_{1q} \end{bmatrix} = \begin{bmatrix} 0 & \omega C \\ -\omega C & 0 \end{bmatrix} \begin{bmatrix} v_{pccd} \\ v_{pccq} \end{bmatrix} - \begin{bmatrix} C & 0 \\ 0 & C \end{bmatrix} \frac{d}{dt} \begin{bmatrix} v_{pccd} \\ v_{pccq} \end{bmatrix} + \begin{bmatrix} i_{2d} \\ i_{2q} \end{bmatrix} \quad (3)$$

where i_2 represents the current from the wind power collector and C represents the capacitance seen at the PCC point. The voltage controller in the *dq* reference frame which produces the *dq* current references is described as

$$\begin{cases} i_{1d}^* = i_{2d} + \omega C v_{pccq} - \left[k_{vp}(v_{pccd}^* - v_{pccd}) + k_{vi}\int (v_{pccd}^* - v_{pccd})dt\right] \\ i_{1q}^* = i_{2q} - \omega C v_{pccd} - \left[k_{vp}(v_{pccq}^* - v_{pccq}) + k_{vi}\int (v_{pccq}^* - v_{pccq})dt\right] \end{cases}. \quad (4)$$

3.3 Offshore frequency control

Conventionally, no PLL is used to obtain the offshore frequency and phase angle, as the offshore grid is formed by the offshore station. The offshore frequency f is typically fixed (e.g. 50 Hz) and the phase angle θ is simply derived using the fixed frequency:

$$\theta = 2\pi ft = 100\pi t\,. \quad (5)$$

The MMC station then forms the offshore network according to the phase information obtained by (5) [27]. This approach is easy to implement. However, the offshore frequency flexibility is not utilized and the offshore voltage controllability is compromised.

4 Enhanced AC voltage and frequency control

4.1 Proposed frequency control

A PLL based frequency control is proposed in this section to improve the AC voltage controllability of the MMC station by utilizing the offshore frequency flexibility.

Due to the robustness and ease of implementation, PLL is widely used in tracking the AC voltage angle and frequency [4, 17]. It usually measures the *q*-axis voltage v_{pccq} and a PI regulator drives the offshore frequency in order to obtain zero v_{pccq}, as illustrated in Fig. 3 and (6):

$$f = f_0 + \frac{1}{1 + T_S \cdot s}\left(k_{fp}v_{pccq} + k_{fi}\int v_{pccq}dt\right) \quad (6)$$

where T_s is the time constant of low pass filter (LPF) and is set at 0.1 s in this paper.

The proposed offshore MMC frequency control loop considers such operating principle of the PLL and uses a frequency / *q*-axis voltage droop for regulating the offshore AC frequency f through v^*_{pccq} as:

$$v_{pccq}^* = K(f^* - f) \quad (7)$$

where K is the droop gain and f^* is the frequency reference. When $f < f^*$, the frequency loop as shown (7) outputs positive v^*_{pccq} and feeds to the AC voltage loop. The AC voltage control loop regulates the MMC output v_{pccq} to follow the positive reference v^*_{pccq} and thus $v_{pccq} > 0$. Consequently, the produced voltage at the PCC will lead the *d*-axis voltage as show in Fig. 3. The positive v_{pccq} is then detected by the PLL and the measured frequency f increases, as depicted by (6), and so as the frequency of the generated offshore AC voltage. Similarly, if $f > f^*$, a negative voltage v_{pccq} is generated by the MMC at the PCC. Under such a

This paper is a post-print of a paper submitted to and accepted for publication in IET Renewable Power Generation and is subject to Institution of Engineering and Technology Copyright. The copy of record is available at IET Digital Library.

condition, the frequency detected by the PLL reduces due to the negative voltage ($v_{pccq} < 0$) and so as the frequency of the MMC AC output. Therefore, with the proposed frequency control, the offshore frequency f can be tightly controlled at the reference value.

Besides voltage and current control loop, an additional frequency loop is proposed in this paper for the MMC station to improve the offshore AC voltage controllability. As aforementioned, the additional PLL contributes to the fast offshore network angle tracking and actively sets the q-axis voltage. By effectively utilizing the flexibility of the q-axis voltage, the proposed frequency loop acts to lock a new grid angle during disturbance (e.g. sudden power and voltage changes) and helps the system find a new operation point, which stabilizes the offshore voltage and yields improved system dynamics, as will be demonstrated in Section 5.

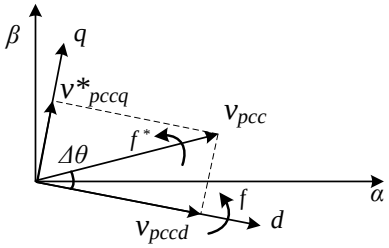

Fig 3. *Synchronization control.*

4.2 Fault current providing capability of the offshore MMC

In the event of an offshore AC fault, the offshore voltage drops and the offshore MMC station needs to limit the AC current whereas a certain fault current is also required for offshore AC protection purpose.

4.2.1 Fault current providing control

After an offshore AC fault, MMC_1 initially tries to restore the AC voltage by reducing d-axis current i_{1d} (due to the existence of the outer AC voltage loop). However, when the offshore AC voltage is significantly reduced, e.g. around to zero, no active power can be generated and transmitted during the fault. i_{1d} is thus limited at around zero. To provide sufficient fault current for the protection relays connected to the wind turbine clusters, the q-axis current reference of the offshore MMC station i^*_{1q} is modified accordingly as shown in Fig. 4. The difference between v_{pccd} and v^*_{pccd} (v^*_{pccd}-v_{pccd}) is measured and compared to the pre-set threshold, e.g. 0.4 pu. During normal operation, v^*_{pccd} - v_{pccd} is less than the threshold and i^*_{1q} is set by the q-axis voltage control loop. However, during an offshore AC fault, v_{pccd} is significantly reduced and the d-axis voltage error will be over the threshold. Thus, an additional component Δi_q is added to the reference to regulate the q-axis current and inject fault current for the offshore network. The fault current profile is illustrated in Fig. 4. After the offshore AC fault, the fault current i_2 provided by the offshore MMC is gradually ramped up from 0.3 pu with the rate of 0.9 pu/s until fault clearance. With the fault current profile defined by Fig. 4, offshore breakers are opened by overcurrent protection while the potential large capacity requirements of circuit breakers are avoided. To provide a maximum fault current of 1.2 pu, the gain k_f between (v^*_{pccd}-v_{pccd}) and Δi_q is set at 3 (1.2/0.4=3) in this paper.

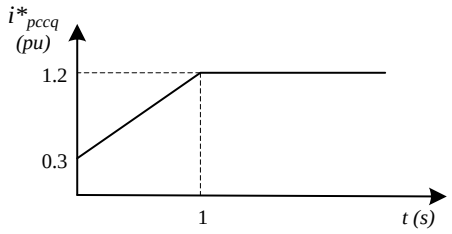

Fig 4. *Fault current supply.*

4.2.2 Offshore AC fault protection

By measuring overcurrent and properly setting the thresholds, the offshore AC fault can be accurately located and the corresponding circuit breaker is selectively opened to isolate the fault. Although MMC and WT converters have limited fault current capability (e.g. maximum 1.2 pu), during an offshore fault, substantial overcurrent will still be present as all the converters will feed fault current to the fault.

Considering the fault on Cable 1 (F1, Fig. 1), the offshore AC voltage rapidly drops to zero after the fault. Fault currents from the offshore MMC_1 station and WTs at clusters 2 and 3 flow through breaker CB_1, as:

$$i_{CB1} = i_2 - i_{wt2} - i_{wt3}. \tag{8}$$

With the increase of fault currents as defined in Fig. 4, the current flowing through CB_1 gradually increases and can be much higher than the nominal current. Thus, overcurrent protection can be adopted to open CB_1 and isolate the fault. The breakers on the healthy cables CB_2 and CB_3 do not experience overcurrent and thus remain closed:

$$i_{CB2} = i_{wt2}, \qquad i_{CB3} = i_{wt3}. \tag{9}$$

Thus, for protection of cluster cable fault, overcurrent protection provides a relatively simple and reliable approach for the WTs.

4.2.3 SM capacitance requirements

Compared to normal operation, the fault current providing capability of the offshore MMC station requires relatively larger SM capacitance, which will be described in this subsection.

This paper is a post-print of a paper submitted to and accepted for publication in IET Renewable Power Generation and is subject to Institution of Engineering and Technology Copyright. The copy of record is available at IET Digital Library.

The arm voltage v_{arm} of the MMC station is given as [8]

$$v_{arm}(\omega t)=\sqrt{\frac{2N\bullet\Delta E_{arm}(\omega t)}{C_{SM}}+V_{dc}^{\ 2}} \tag{10}$$

where N is the submodule (SM) number per arm; C_{SM} is the SM capacitance; ΔE_{arm} is the arm energy variation; V_{dc} is the DC voltage. With third harmonic injection, ΔE_{arm} is expressed as (11) whose last part shows the influence of the third harmonic on the arm energy variation in the fault current providing control [28]:

$$\begin{aligned}\Delta E_{arm}(\omega t)&=\frac{1}{\omega}\int_0^{\omega t}v_{arm}i_{arm}d(\omega t)=\frac{V_{dc}I_m}{4\omega}\left[\cos\varphi-\cos(\omega t-\varphi)\right]\\&-\frac{V_mI_{dc}}{3\omega}\left[1-\cos(\omega t)\right]+\frac{V_mI_m}{8\omega}\left[\sin(2\omega t-\varphi)+\sin\varphi\right]\\&\underbrace{-\frac{V_{3m}I_m}{4\omega}\left\{\frac{1}{2}\sin(2\omega t+\varphi)-\frac{1}{4}\sin(4\omega t-\varphi)-\frac{1}{4}\sin\varphi+\frac{4I_{DC}}{9I_m}\left[1-\cos(3\omega t)\right]\right\}}_{\text{third harmonic influence}}\end{aligned} \tag{11}$$

where i_{arm} is the arm current; V_m and I_m are the phase voltage and current amplitudes respectively; V_{3m} is the amplitude of third harmonic voltage; I_{dc} is the DC current; and φ is the phase angle difference between the voltage and current on the MMC AC side.

From (10) and (11), the arm voltage is illustrated in Fig. 5. With the equivalent capacitor discharging time constant setting at 30 ms (30 kJ/MVA), the arm voltage is well regulated in the range of ±10% [29]. After a solid offshore AC fault at t=0.1 s, the offshore voltage drops to zero and the MMC station starts to provide q-axis current to enable fault detection. The arm voltage variation then increases and is 1.44 times that of normal operation. Thus, to provide the fault current, relatively large SM capacitance is required, which can be designed according to (10) and (11).

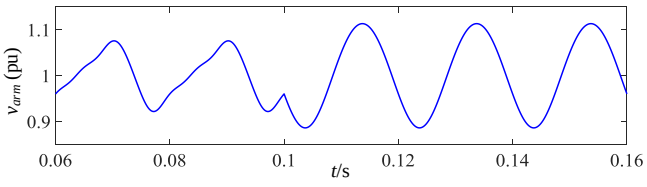

Fig. 5. *Arm voltage of MMC, where the offshore station provides q-axis current to enable fault detection after an offshore AC fault at t=0.1 s.*

4.3 Offshore AC voltage control for onshore AC fault ride-through operation

After a solid onshore three-phase fault, the onshore grid voltage drops to around zero and thus the active power that can be transmitted by the onshore MMC station is significantly reduced. Meanwhile, the WTs still try to transmit power to the HVDC-link and the resultant power surplus leads to the increase of the HVDC link voltage. To alleviate the DC overvoltage, the offshore MMC station needs to immediately reduce power absorption from the offshore network and the power generation from the WTs also needs to be rapidly reduced.

To achieve this, the offshore grid voltage is reduced immediately after detecting DC overvoltage using an HVDC voltage dependent offshore AC voltage controller which is introduced to actively regulate the offshore voltage and ride-through the onshore fault, as shown in Fig. 2 and Fig. 6. The DC voltage V_{dc} and offshore AC voltage v^*_{pccd} are controlled at the rated value $V_{dcrated}$ and $V_{acrated}$ respectively during normal operation. Once V_{dc} is over the lower threshold V_{thl} after an onshore fault, the offshore voltage v^*_{pccd} starts to reduce according to the solid curves defined in Fig. 6 and (12):

$$v^*_{pccd}=\begin{cases}V_{acrated}, & V_{dc}\le V_{thl}\\ \dfrac{V_{acrated}}{V_{thl}-V_{thu}}(V_{dc}-V_{thu}), & V_{thl}<V_{dc}\le V_{thu}\\ 0, & V_{thu}<V_{dc}\end{cases}. \tag{12}$$

The offshore AC voltage v^*_{pccd} is decreased to zero when the DC voltage reaches the upper threshold V_{thu} and thus the power injected to the HVDC-link and generated by the WTs are all reduced to zero.

After fault clearance (typically several tens ms), the onshore MMC station resumes DC voltage control capability and the overvoltage on HVDC-link starts to reduce and the system gradually restores. When the DC voltage reaches the lower threshold V_{thl}, the offshore voltage v^*_{pccd} is gradually restores governed by the dashed curve in Fig. 6 and (13). The lower and upper thresholds V_{thl} and V_{thu} are set at 1.05 pu and 1.15 pu respectively in this paper.

$$v^*_{pccd}=\begin{cases}0, & V_{thl}<V_{dc}\\ \dfrac{V_{acrated}}{V_{dcrated}-V_{thl}}(V_{dc}-V_{thl}), & V_{dcrated}<V_{dc}\le V_{thl}\\ V_{acrated}, & V_{dc}\le V_{dcrated}\end{cases}. \tag{13}$$

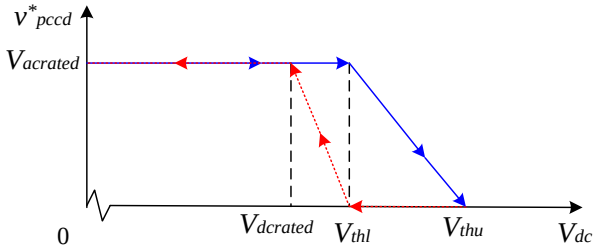

Fig. 6. *Characteristics of the HVDC voltage dependent offshore AC voltage.*

5 Simulation results

The proposed control strategy of the offshore station MMC_1 is tested in Matlab/Simulink environment using the model shown in Fig. 1, where the generator-side WT converters are represented by DC voltage sources for

This paper is a post-print of a paper submitted to and accepted for publication in IET Renewable Power Generation and is subject to Institution of Engineering and Technology Copyright. The copy of record is available at IET Digital Library.

simplicity. Average-value models are used for the MMC stations [30], and detailed switch model are adopted for the grid-side WT converters. The offshore wind system has three lumped wind turbine models rated at 500 MW, 450 MW, and 50 MW respectively, and connected to the collector buses through 10 km, 5 km and 3 km cables respectively. The detailed parameters of the offshore MMC-HVDC system and the WT converter are listed in Table 1 and Table 2 respectively.

Table 1 Parameters of the MMC-HVDC system

AC grid voltage		429 kV
HVDC voltage		800 kV
MMC power rating		1000 MW
MMC side transformer	Reactance	0.2 pu
	Resistance	0.004452 pu
MMC side AC capacitance		0.01 pu
PCC voltage		200 kV
***R*, *L*, and *C* of Cable**		15 mΩ/km, 0.3 mH/km, 0.12 μF/km

Table 2 Parameters of the lumped wind turbine models

DC voltage of WT converter		65 kV
WT side transformer	Reactance	0.1 pu
	Resistance	0.004 pu
WT side capacitor		0.15 pu
WT side inductor		0.2 pu
***R*, *L*, and *C* of Cable 1 (10km)**		15 mΩ/km, 0.3 mH/km, 0.12 μF/km
***R*, *L*, and *C* of Cable 2 (5km)**		16.5 mΩ/km, 0.33 mH/km, 0.11 μF/km
***R*, *L*, and *C* of Cable 3 (3km)**		150 mΩ/km, 3 mH/km, 0.012 μF/km

5.1 Comparisons on the proposed and conventional controls

5.1.1 Start up

After the stabilization of the HVDC-link voltage regulated by the onshore station MMC_2, the offshore station MMC_1 is enabled at 0.05 s to build the offshore AC voltage. The AC voltage amplitude of the offshore grid during start-up with the conventional and proposed frequency control methods are compared in Fig. 7 (a). With the proposed control, the *d*-axis voltage v_{pccd1} follows the reference more tightly than the voltage v_{pccd0} with the fixed frequency conventional control. The three-phase AC voltages and currents at the PCC, as well as the frequency response with the proposed control are displayed in Fig. 7 (b), (c), and (d) respectively.

By utilizing the offshore frequency flexibility, the proposed strategy tightly controls the AC voltage of the offshore network compared to conventional approach with fixed offshore frequency. This contributes to a stable transmission of the offshore wind energy.

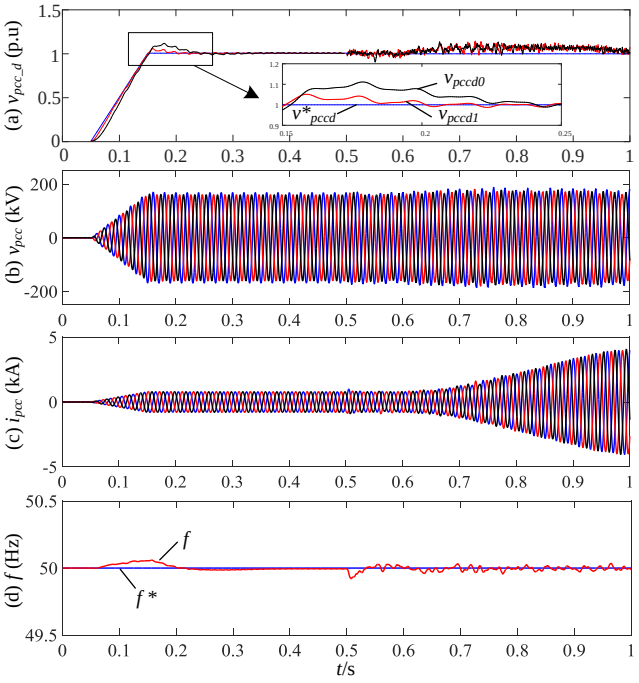

Fig. 7. *Simulation waveforms of offshore station MMC_1 during start-up and wind energy ramping.*

(a) Comparison of d-axis PCC voltage with different control strategies, (b) three-phase PCC voltages, (c) three-phase currents, (d) offshore frequency.

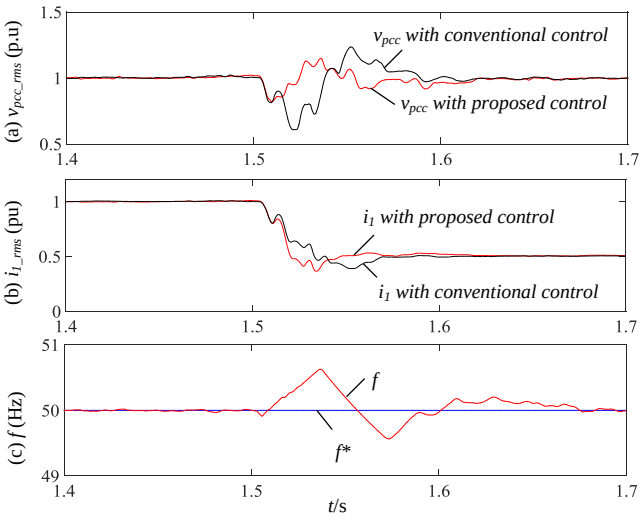

Fig.8. *Voltage and current comparison during power step.*

(a) PCC RMS voltages, (b) MMC_1 RMS currents, (c) offshore frequency.

At 0.5 s, all the three lumped wind turbines are connected into the transmission system and start to generate power from 0.6 s, 0.65 s, and 0.7 s respectively. The voltage amplitude at PCC slightly deviates from the reference and

This paper is a post-print of a paper submitted to and accepted for publication in IET Renewable Power Generation and is subject to Institution of Engineering and Technology Copyright. The copy of record is available at IET Digital Library.

fast restores after the power reaches the rated value, Figs. 5 (a) and (b). As shown in Figs. 5 (c) and (d), the AC currents of the offshore station MMC_1 increase with the increase of the power and the offshore frequency is tightly regulated around the reference during the start-up, benefitting from the proposed frequency control. After t=0.95 s, the power generated by the three wind turbines reaches to the rated value and the offshore MMC operates in steady state and transmits rated power to the onshore side.

5.1.2 Power step

To further demonstrate the advantages of the proposed control over conventional method, the offshore voltages and currents during power step are compared in Fig. 8. At t=1.5 s, VSC_1 is suddenly disconnected with the offshore network and the wind power is reduced from 1 pu to 0.5 pu. The offshore AC voltage fluctuates following the power step. With the proposed control, the offshore voltage restores faster than that with conventional control, as shown in Fig. 8 (a). Similarly, the current of the offshore MMC station experiences less disturbance and exhibits better dynamic response with the proposed scheme, as displayed in Fig. 8 (b).

5.2 Offshore AC fault ride-through operation

The performance of the proposed control is also assessed during an offshore AC fault. The current waveforms in Fig. 9 shows in per unit values based on the respect power of each string/converter. At t=1.15 s, a symmetrical offshore AC fault F1 is applied at Cable 1 as shown in Fig. 1 and the offshore AC voltage rapidly drops to around zero. As the voltage on PCC cannot follow the reference, MMC_1 reverses the power flow to try to restore the voltage, leading to saturation of the voltage loop. Thus, the offshore MMC_1 provides fault currents, which is gradually ramped from 0.3 pu with the rate of 0.9 pu/s which can be used for fault detection, as shown in Fig. 9 (b) and (e). After fault isolation, the AC voltage of the offshore network gradually restores to the rated value by MMC_1 as shown in Fig. 9 (a). The offshore frequency is regulated and restores to the reference value after the fault isolation, Fig. 9 (c).

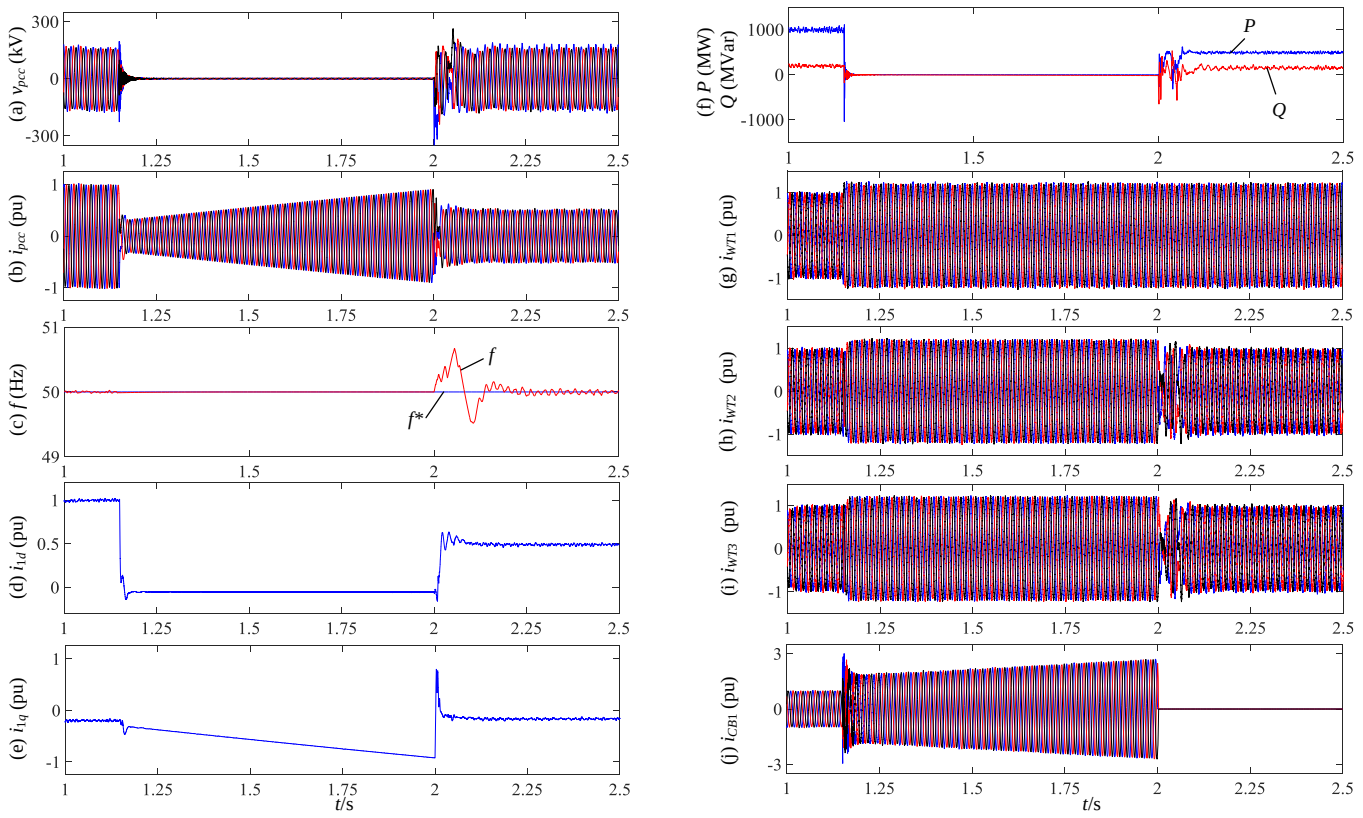

Fig. 9. *Simulation waveforms during offshore AC fault.*

(a) PCC three-phase voltages, (b) MMC_1 three-phase currents, (c) offshore frequency, (d) MMC_1 d-axis current, (e) MMC_1 q-axis current, (f) MMC_1 real and reactive power, (g) three-phase currents of WT_1, (h) three-phase currents of WT_2, (i) three-phase currents of WT_3, (j) three-phase currents of circuit breaker CB_1.

This paper is a post-print of a paper submitted to and accepted for publication in IET Renewable Power Generation and is subject to Institution of Engineering and Technology Copyright. The copy of record is available at IET Digital Library.

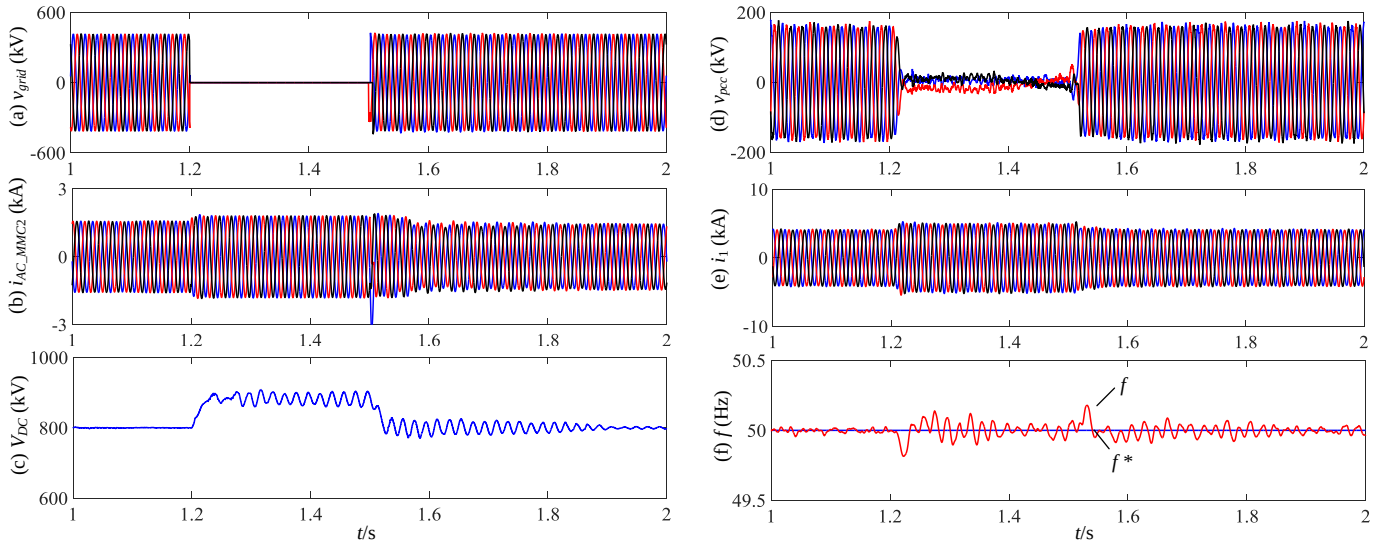

Fig. 10. *Simulation waveforms during onshore fault occurs.*

(a) Onshore grid voltages, (b) three-phase currents of MMC_2, (c) DC voltage of HVDC transmission line, (d) three-phase voltages on PCC bus, (e) three-phase currents of MMC_1, (f) offshore frequency.

Fig. 9 (g) to (j) displays the currents of the three lumped wind turbines during the offshore AC fault. The output currents of the three lumped turbines rapidly increase and hit the current limit after the fault at t=1.15 s. As shown in Fig. 9 (j), the fault currents provided by MMC_1 is gradually ramped up and the fault currents flowing through the circuit breaker on the faulty branch (CB_1, Fig. 1) reach the protection threshold at t= 1.95 s, and thus CB_1 is commanded to open to isolate the faulty branch. During the fault period from 1.15 s to 2 s, all three wind turbines limit the fault currents and once the fault at Cable 1 is clear, currents on Cables 2 and 3 are quickly recovered to their rated values. In the simulation and for illustration purpose, WT_1 (VSC_1) remains operational (operating at current limit) although Cable 1 has been disconnected by CB_1 after 2 s.

With the proposed control scheme, the whole offshore system is still well controlled during such serious offshore AC fault and can restore normal operation automatically.

5.3 Onshore AC fault ride-through operation

To test the proposed control in the event of an onshore AC fault, a symmetrical solid fault F2 is applied at the AC-side of the onshore station MMC_2 as illustrated in Fig. 1 at t=1.2 s and is cleared after 0.3 s.

As shown in Fig. 10 (a) and (b), the onshore voltage drops to zero after the fault and the onshore MMC_2 operates on current limiting mode to support the AC grid. As the output power of MMC_2 is reduced to zero and the offshore wind energy is still imported to HVDC-link, the DC voltage increases, which triggers the offshore fault protection controller. As displayed in Fig. 10 (c) and (d), the offshore voltage is actively decreased according to the profile defined in Fig. 6, which reduces the imported power to the HVDC-link and the HVDC voltage is limited less than 1.2 pu. During the fault, the offshore station MMC_1 operates on current limiting mode and the offshore frequency is welled regulated around 50 Hz as shown in Fig. 10 (e) and (f).

After fault clearance, the power transmission of the onshore MMC_2 restores and the DC voltage drops to 1.05 pu at 1.54 s. The offshore AC voltage then increases according to (13) and the system autonomously restores normal operation without any communication.

6 Conclusion

This paper proposes an enhanced frequency and AC voltage control scheme of the offshore MMC station for wind energy transmission. An additional frequency loop is proposed to set the q-axis voltage reference to control the offshore network frequency. Compared to conventional method without frequency loop, the proposed scheme improves the controllability of the offshore AC voltage and contributes to stable offshore wind energy transmission. A fault current injection control is then proposed, where the offshore MMC station actively provides fault currents to enable overcurrent protection for the offshore network. To ride-through onshore AC faults, a DC voltage dependent AC voltage profile is introduced to actively reduce the offshore AC voltage and alleviate the overvoltage of the HVDC cables. Simulation results demonstrate the effectiveness of the proposed control considering normal operation, offshore AC fault, and onshore AC fault.

This paper is a post-print of a paper submitted to and accepted for publication in IET Renewable Power Generation and is subject to Institution of Engineering and Technology Copyright. The copy of record is available at IET Digital Library.

Acknowledgements

This study is supported in part by the State Key Laboratory of Alternate Electrical Power System with Renewable Energy Sources (Grant No. LAPS17010)

References

[1] J. Lv, P. Dong, G. Shi, X. Cai, H. Rao, and J. Chen, "Subsynchronous oscillation of large DFIG-based wind farms integration through MMC-based HVDC," in *2014 International Conference on Power System Technology*, 2014, pp. 2401-2408.

[2] R. Vidal-Albalate, H. Beltran, A. Rolán, E. Belenguer, R. Peña, and R. Blasco-Gimenez, "Analysis of the Performance of MMC Under Fault Conditions in HVDC-Based Offshore Wind Farms," *IEEE Transactions on Power Delivery*, vol. 31, pp. 839-847, 2016.

[3] O. G. B. M. Raza, "Multi-Infeed Control of VSC-HVDC Transmission System for Offshore Wind Power Plant Integration," presented at the 13th Wind Integration Workshop, Berlin Germany, 2014.

[4] M. Saeedifard and R. Iravani, "Dynamic performance of a modular multilevel back-to-back HVDC system," in *2011 IEEE Power and Energy Society General Meeting*, 2011, pp. 1-1.

[5] N. Ahmed, A. Haider, D. V. Hertem, L. Zhang, and H. P. Nee, "Prospects and challenges of future HVDC SuperGrids with modular multilevel converters," in *Proceedings of the 2011 14th European Conference on Power Electronics and Applications*, 2011, pp. 1-10.

[6] L. Zhang, L. Harnefors, and H. P. Nee, "Modeling and Control of VSC-HVDC Links Connected to Island Systems," *IEEE Transactions on Power Systems*, vol. 26, pp. 783-793, 2011.

[7] P. Wang, X. P. Zhang, P. F. Coventry, and R. Zhang, "Start-Up Control of an Offshore Integrated MMC Multi-Terminal HVDC System With Reduced DC Voltage," *IEEE Transactions on Power Systems*, vol. 31, pp. 2740-2751, 2016.

[8] R. Zeng, L. Xu, L. Yao, and B. W. Williams, "Design and Operation of a Hybrid Modular Multilevel Converter," *IEEE Transactions on Power Electronics*, vol. 30, pp. 1137-1146, 2015.

[9] L. Zhang, L. Harnefors, and H. P. Nee, "Interconnection of Two Very Weak AC Systems by VSC-HVDC Links Using Power-Synchronization Control," *IEEE Transactions on Power Systems*, vol. 26, pp. 344-355, 2011.

[10] S. Debnath and M. Chinthavali, "Control of MMC-HVDC in low-inertia weak grids," in *2017 IEEE 12th International Conference on Power Electronics and Drive Systems (PEDS)*, 2017, pp. 435-441.

[11] B. Liu, J. Xu, R. E. Torres-Olguin, and T. Undeland, "Faults mitigation control design for grid integration of offshore wind farms and oil & gas installations using VSC HVDC," in *SPEEDAM 2010*, 2010, pp. 792-797.

[12] L. Xu, L. Yao, and C. Sasse, "Grid Integration of Large DFIG-Based Wind Farms Using VSC Transmission," *IEEE Transactions on Power Systems*, vol. 22, pp. 976-984, 2007.

[13] U. Karaagac, L. Cai, and J. Mahseredjian, "Simulation of startup sequence of an offshore wind farm with MMC-HVDC grid connection," in *2017 IEEE Power & Energy Society General Meeting*, 2017, pp. 1-1.

[14] M. Amin, A. Rygg, and M. Molinas, "Self-Synchronization of Wind Farm in an MMC-Based HVDC System: A Stability Investigation," *IEEE Transactions on Energy Conversion*, vol. 32, pp. 458-470, 2017.

[15] J. Lyu, X. Cai, and M. Molinas, "Frequency Domain Stability Analysis of MMC-Based HVdc for Wind Farm Integration," *IEEE Journal of Emerging and Selected Topics in Power Electronics*, vol. 4, pp. 141-151, 2016.

[16] U. Karaagac, J. Mahseredjian, L. Cai, and H. Saad, "Offshore wind farm modeling accuracy and efficiency in MMC-based multi-terminal HVDC connection," in *2017 IEEE Power & Energy Society General Meeting*, 2017, pp. 1-1.

[17] J. Svensson, "Synchronisation methods for grid-connected voltage source converters," *IEE Proceedings - Generation, Transmission and Distribution*, vol. 148, pp. 229-235, 2001.

[18] H. Zhang, D. Flórez, C. Saudemont, and F. Gruson, "Improved overvoltage limitation control approach of a DC series offshore wind farm based on MMC," in *2016 18th Mediterranean Electrotechnical Conference (MELECON)*, 2016, pp. 1-6.

[19] W. Wang, Y. Li, Y. Cao, U. Häger, and C. Rehtanz, "Adaptive Droop Control of VSC-MTDC System for Frequency Support and Power Sharing," *IEEE Transactions on Power Systems*, vol. 33, pp. 1264-1274, 2018.

[20] K. Schönleber, E. Prieto-Araujo, S. Ratés-Palau, and O. Gomis-Bellmunt, "Extended Current Limitation for Unbalanced Faults in MMC–HVDC–connected Wind Power Plants," *IEEE Transactions on Power Delivery*, vol. PP, pp. 1-1, 2017.

[21] J. N. Sakamuri, M. Altin, A. D. Hansen, and N. A. Cutululis, "Coordinated frequency control from offshore wind power plants connected to multi

This paper is a post-print of a paper submitted to and accepted for publication in IET Renewable Power Generation and is subject to Institution of Engineering and Technology Copyright. The copy of record is available at IET Digital Library.

terminal DC system considering wind speed variation," *IET Renewable Power Generation*, vol. 11, pp. 1226-1236, 2017.

[22] Y. Yu, Z. Xu, and T. An, "Fault ride-through strategy for fully rated converter wind turbines connected to the grid via MMC-HVDC transmission," in *12th IET International Conference on AC and DC Power Transmission (ACDC 2016)*, 2016, pp. 1-5.

[23] S. Cao, W. Xiang, L. Yao, B. Yang, and J. Wen, "AC and DC fault ride through hybrid MMC integrating wind power," *The Journal of Engineering*, vol. 2017, pp. 828-833, 2017.

[24] S. Bernal-Perez, S. Ano-Villalba, R. Blasco-Gimenez, and J. Rodriguez-D'Derlee, "Efficiency and Fault Ride-Through Performance of a Diode-Rectifier- and VSC-Inverter-Based HVDC Link for Offshore Wind Farms," *IEEE Transactions on Industrial Electronics*, vol. 60, pp. 2401-2409, 2013.

[25] U. Karaagac, J. Mahseredjian, L. Cai, and H. Saad, "Offshore Wind Farm Modeling Accuracy and Efficiency in MMC-Based Multiterminal HVDC Connection," *IEEE Transactions on Power Delivery*, vol. 32, pp. 617-627, 2017.

[26] J. N. Sakamuri, Z. H. Rather, J. Rimez, M. Altin, G. Ö, and N. A. Cutululis, "Coordinated Voltage Control in Offshore HVDC Connected Cluster of Wind Power Plants," *IEEE Transactions on Sustainable Energy*, vol. 7, pp. 1592-1601, 2016.

[27] Y. Li, Z. Xu, J. Østergaard, and D. J. Hill, "Coordinated Control Strategies for Offshore Wind Farm Integration via VSC-HVDC for System Frequency Support," *IEEE Transactions on Energy Conversion*, vol. 32, pp. 843-856, 2017.

[28] R. Li, J. E. Fletcher, L. Xu, and B. W. Williams, "Enhanced Flat-Topped Modulation for MMC Control in HVDC Transmission Systems," *IEEE Transactions on Power Delivery*, vol. 32, pp. 152-161, 2017.

[29] R. Li, L. Xu, L. Yao, and B. W. Williams, "Active Control of DC Fault Currents in DC Solid-State Transformers During Ride-Through Operation of Multi-Terminal HVDC Systems," *IEEE Transactions on Energy Conversion*, vol. 31, pp. 1336-1346, 2016.

[30] F. B. Ajaei and R. Iravani, "Enhanced Equivalent Model of the Modular Multilevel Converter," *Power Delivery, IEEE Transactions on*, vol. 30, pp. 666-673, 2015.